Editors' Suggestion | Featured in Physics

Resonant Nanopumps: ac Gate Voltages in Conical Nanopores Induce Directed Electrolyte Flow

Aaron D. Ratschow,[1] Doyel Pandey,[2] Benno Liebchen,[3,*] Somnath Bhattacharyya,[2] and Steffen Hardt[1,†]
[1]Institute for Nano- and Microfluidics, TU Darmstadt, Alarich-Weiss-Straße 10, D-64237 Darmstadt, Germany
[2]Department of Mathematics, Indian Institute of Technology Kharagpur, Kharagpur, West Bengal, India–721302
[3]Theory of Soft Matter, Department of Physics, TU Darmstadt, Hochschulstraße 12, D-64289 Darmstadt, Germany

(Received 15 July 2022; revised 27 September 2022; accepted 10 November 2022; published 22 December 2022; corrected 5 December 2023)

Inducing transport in electrolyte-filled nanopores with dc fields has led to influential applications ranging from nanosensors to DNA sequencing. Here we use the Poisson-Nernst-Planck and Navier-Stokes equations to show that unbiased ac fields can induce comparable directional flows in gated conical nanopores. This flow exclusively occurs at intermediate driving frequencies and hinges on the resonance of two competing timescales, representing space charge development at the ends and in the interior of the pore. We summarize the physics of resonant nanopumping in an analytical model that reproduces the results of numerical simulations. Our findings provide a generic route toward real-time controllable flow patterns, which might find applications in controlling the translocation of small molecules or nanocolloids.

DOI: 10.1103/PhysRevLett.129.264501

Introduction.—In the past few years, nanochannels and nanopores have been the subject of rapidly intensifying research activities. They have found applications as nanosensors [1,2], in DNA sequencing [3,4], for liquid and gas-phase separation processes [5], for water desalination by reverse osmosis [6], or for power generation from salinity gradients [7]. For many applications of electrolyte-filled nanochannels and nanopores, it is desirable to control the transport processes within. For such purposes, control schemes based on a gate voltage, often applied via a gate electrode, have been developed. By tuning the gate voltage, the electrostatic potential at the channel or pore walls can be modulated. In turn, the charge in the diffuse part of the electric double layer (EDL) can be controlled, which is especially interesting in the case of overlapping EDLs. In experiments it was demonstrated that corresponding schemes enable controlling the transport properties of nanopores. Examples include the control of water permeation [8] and DNA translocation [9–11], and more generally, the control of electromigration and diffusion fluxes through nanopores [12–17] which can even be rectified [18–21]. As for the latter, employing nanopores with conical or converging geometries has proven particularly useful [22–24]. For example, when filled with an electrolyte solution, their electric resistance can become direction dependent, giving such pores current-rectifying properties [25–27] with asymmetric current-voltage $I(V)$ curves [28]. Notably, to date, most existing transport control and rectification schemes in nanopores employ a dc (or slow ac) driving, based on a constant applied voltage, such that transport is essentially controlled by the equilibrium or steady-state properties of the system. In microfluidics, however, it was shown that flow can be induced by dynamic charging of thin EDLs over flat, periodic electrode arrays with broken symmetry [29].

In the present Letter, we explore the transport properties of conical nanopores under the influence of ac driving, i.e., for gate electrodes energized with frequencies high enough to keep the ion cloud in the pore persistently away from its equilibrium. By combining simulations of the Poisson-Nernst-Planck and Navier-Stokes equations, whose fundamental validity in comparison to molecular simulations has been demonstrated down to pore diameters of a few nanometers [30,31], and analytical modeling, we show that an ac driving induces a novel and subtle transport mechanism in which the pore serves as a nanopump creating a net fluid flow—even in the absence of a direction-dependent flow resistance. Remarkably, the pumping neither occurs for very slow nor very fast driving, but the maximum flow rate is reached at a characteristic resonance frequency which can be determined by the system's intrinsic response to a voltage step. We call this mechanism resonant nanopumping. In contrast to previously reported pumping mechanisms that rely on the coupling of translational and rotational molecular degrees of freedom under ac driving [32,33], our mechanism is completely based on continuum-mechanical concepts. We explain it using an analytical model which predicts the multidimensional parametric dependency of the flow rate, in quantitative agreement with our detailed simulations. Note in particular that such a transport mechanism at the nanoscale must overcome challenges not present at larger

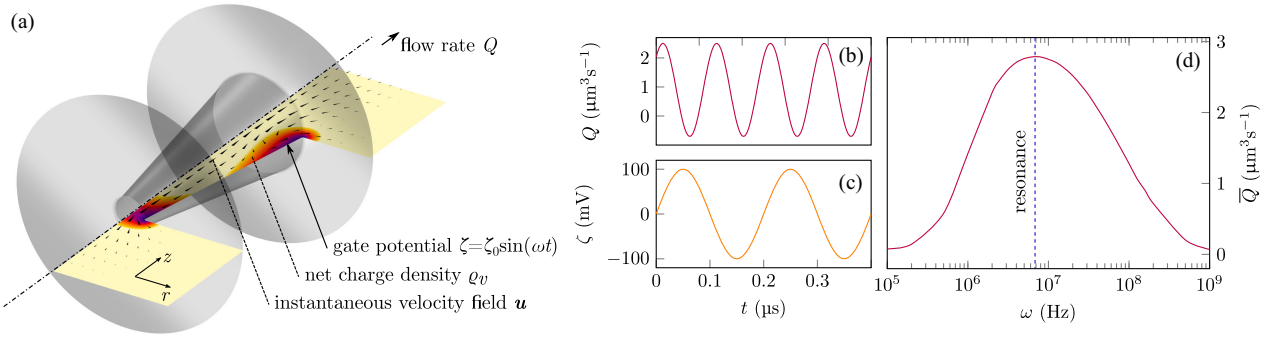

FIG. 1. Resonant nanopumping. (a) Schematic illustration of the conical nanopore connecting two reservoirs (indicated by gray disks), the flow field (arrows), and the charge density [colors, ranging from low (yellow) to high (purple) charge density]. (b)–(d) Applying an unbiased ac gate potential ζ with a frequency ω (c) to the pore wall leads to a flow Q that oscillates with 2ω and is biased toward the wide end of the pore (b). The magnitude of the mean flow $\bar{Q}$ strongly depends on ω, with a distinct resonant behavior (d).

scales. (i) There is no "bulk" region within a nanopore, so that charges need to enter and leave the pore through the openings at the pore ends. (ii) The screening layers at the pore walls are not thin compared to the pore diameter and may even significantly overlap. Thus, while pioneering earlier work [29] hinges on the assumption of thin Debye layers and the existence of a bulk region above the electrode and, accordingly, has little predictive power for gated nanopores, the mechanism which we propose creates an efficient, controllable, and predictable transport at the nanoscale. In addition, we note that the present Letter links the physics of nanopores to Brownian ratchets [34–36], in the sense that the creation of directed transport relies on the same three generic ingredients, which are (i) time-reversal symmetry breaking, (ii) parity symmetry breaking, and (iii) a persistent driving creating a persistent nonequilibrium situation [37].

Setup.—We consider a conical nanopore with length $L = 100$ nm, a narrow end radius $r_n = 7.5$ nm, and a half opening angle $\alpha = 10°$, which connects two reservoirs filled with an aqueous, monovalent, binary electrolyte solution (Fig. 1). To avoid singularities, the corners at the two ends of the pore are blunted with a radius of 1 nm. Both reservoirs feature the same prescribed pressure and ion concentrations $c_0 = 3.653$ mM, and their boundaries far from the pore [cropped in Fig. 1(a)] are grounded. The ion concentrations are chosen such that the Debye length λ_D is smaller than r_n. These parameters are used unless stated otherwise. The pore wall is assumed to exhibit no native ζ potential and the gate potential at the wall $\zeta(t)$ can be varied. The pore and reservoir walls [gray in Fig. 1(a)] are considered nonslipping and impermeable for ions.

Flow field.—Let us now explore the flow through the pore when applying an ac gate potential $\zeta(t) = \zeta_0 \sin(\omega t)$ of angular frequency ω. To do this, we numerically solve the fully coupled set of Poisson-Nernst-Planck and Navier-Stokes equations on this axisymmetric two-dimensional geometry using the finite-element method [see Supplemental Material (SM) for details [38]]. We monitor the flow rate $Q = \int_\Gamma u_z dA$ [Figs. 1(b) and 1(d)], with axial velocity u_z at any cross-sectional plane Γ.

When ω tends toward zero, we observe that the time-averaged flow vanishes $\bar{Q} \to 0$ [Fig. 1(d) herein and Movie 1 in SM [38]]. This is plausible, as for slow driving anions and cations alternately enter and leave the pore via both openings and form fully developed EDLs along the entire pore wall over the full driving cycle (Fig. 2, left-hand panel). Consequently, the electric body force within the equilibrium EDLs is counteracted by the electrohydrostatic (osmotic) pressure gradient and the net force on the fluid vanishes at all times [41]. Similarly, when ω tends toward infinity, we observe a rapidly oscillating but very weak flow Q, and $\bar{Q}$ again tends toward zero [Fig. 1(d) herein and Movie 2 in SM [38]]. The reason is that for very fast driving, ions are alternately driven toward and away from the pore wall to screen the gate potential, but do not have

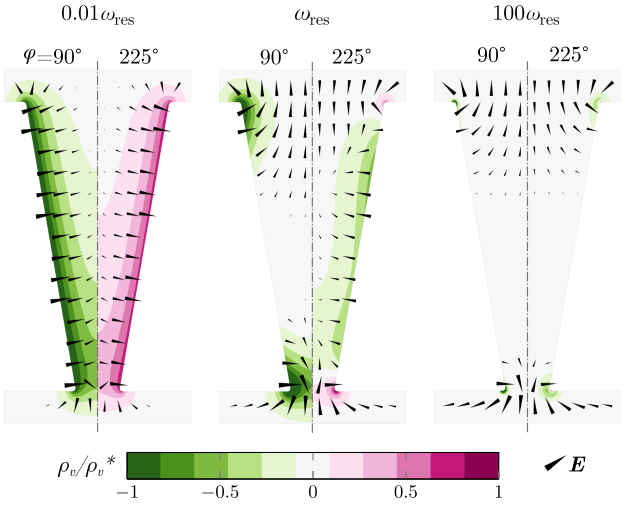

FIG. 2. Net charge density ρ_v and electric field vectors $\boldsymbol{E}$ within the nanopore for slow, resonant, and fast driving with $\zeta = \zeta_0 \sin(\omega t)$. The scales ρ_v^* are 250, 80, and 20 kC m^{-3}, respectively, $\boldsymbol{E}$ is scaled for optimized visualization. Splits show instantaneous fields at different phase angles $\phi = \omega t$.

enough time to migrate into the pore. Accordingly, we observe small ($\ll \lambda_D$) charged regions at the corners, whereas the liquid around the pore center remains uncharged (Fig. 2, right-hand panel). In this case, charged regions are virtually absent and the flow is very weak. Remarkably, however, for intermediate ω, we observe a significant flow. It oscillates with twice the driving frequency and shows a strong bias, with net flow $\bar{Q}$ from the narrow to the wide pore end [Fig. 1(b) herein and Movie 3 in SM [38]]. The emergence of such a flow might be a surprise, since there are no apparent driving gradients, especially pressure gradients, induced by the boundary conditions. To understand how this flow comes about, note that after each sign change of the gate potential, new EDLs start to form at both pore ends and spread toward the pore center. This process gets interrupted by the subsequent sign change of the gate potential such that the EDLs follow the gate potential with a delay, causing charge density gradients along the pore that result in significant axial electric fields at the pore ends. The middle panel of Fig. 2 even shows the simultaneous presence of oppositely charged regions. These axial electric fields exert a body force $\rho_v \boldsymbol{E}$ on the charged liquid at the corners that oscillates with twice the driving frequency 2ω, since both the charge density ρ_v and the electric field $\boldsymbol{E}$ oscillate with ω. Because of the conical pore shape, these body forces asymmetrically push fluid into the pore, leading to the observed bias which we will further discuss and quantify below.

Step response and characteristic timescales.—To understand the complex interplay of space charge and electric field, we explore the response of the system (in equilibrium at $t = 0$) to a steplike gate potential $\zeta(t) = \Theta(t)\zeta_0$, where $\Theta(t) = 1$ for $t \geq 0$ and zero elsewise (step response method [42]). Such a gate potential causes a fast increase of the flow rate toward a distinct maximum, followed by a comparatively slow relaxation toward the new equilibrium state [see Fig. 4(a)]. That is, the system possesses two competing inherent timescales: a short one corresponding to the time needed for developing EDLs at the corners and a long timescale corresponding to the time needed for ions to migrate into the pore and develop an EDL throughout. Within the latter timescale, the axial electric field vanishes, ultimately leading to a wall-normal electric field in all space-charge regions (Fig. 3, left-hand splits).

Viewing one pore end independently, the only length scale that the electric field can depend on is the pore diameter. Thus, after switching on the gate potential at $t = 0$, there is a significant axial electric field which essentially persists over that length scale (Fig. 3, left-hand and middle panels). Since the interaction of charges with this field drives the flow, we identify the short timescale as the time of diffusive transport of counterions (and co-ions) into (and out of) the pore over a length of one pore diameter to form EDLs at the corners of the pore (Fig. 3, middle panel). Notably, although r_i can be $\sim\lambda_D$ in this Letter, we find that the charging timescale for a pore end largely

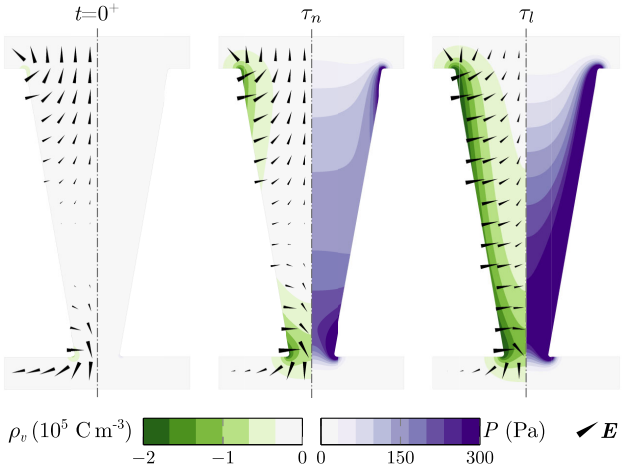

FIG. 3. Net charge density ρ_v with electric field vectors $\boldsymbol{E}$ (left-hand split) and pressure P (right-hand split) right after the gate potential step and after the short and long timescales. An axial pressure gradient quickly develops in response to electric body forces acting at the corners. For long times, equilibrium EDLs form, and the wall-normal electric body force and the pressure gradient cancel.

follows the simple expression

$$\tau_i = 4\frac{\lambda_D r_i}{D}, \qquad i = n, w, \tag{1}$$

obtained for $\lambda_D \ll r_i$ (see Refs. [43,44] and SM [38]). Here D is the ion diffusivity ($= 10^{-9}\ \mathrm{m^2\,s^{-1}}$) and the subscripts n and w denote the narrow and wide ends, respectively.

The long timescale is associated with the filling of the complete pore with counterions, leading to fully evolved EDLs and to a cancellation of the axial electric field. It is the timescale of diffusive transport of ions from both pore ends over a distance of roughly $L/2$, which is derived from the transmission line model as (see Refs. [43,45] and SM [38])

$$\tau_l = \frac{1}{4}\frac{\lambda_D}{\bar{r}}\frac{L^2}{D}, \tag{2}$$

where $\bar{r} = 1/2(r_n + r_w)$ is the mean radius of the conical pore.

Delay effects drive the nanopump.—First, note that for the step response the axial electric body force $\rho_v E_z$ only acts in the time window when ρ_v has already developed and E_z has not yet vanished, i.e., roughly for $t \in [\tau_i, \tau_l]$. Within this time window, the body force pushes liquid into the pore from both ends, irrespective of the sign of ζ. The conical shape breaks the reflection symmetry with respect to z, making the force contributions from both ends unequal. As a result of these localized forces, an axial pressure gradient develops (Fig. 3, right-hand split) and liquid flows from the narrow to the wide end.

Accordingly, when driving the pore with an ac voltage with a frequency large enough to cause significant delay effects, but small enough to allow EDLs to partially

propagate into the pore, we observe unequal oscillating axial body forces at both ends of the pore that drive liquid through it. The mechanism hinges on the two competing charging timescales whose existence has recently been discussed for cylindrical pores [46,47] and is thus not limited to conical shapes.

Analytical model.—To quantitatively predict the flow through the nanopore, we translate the localized axial body force contributions into effective pressures at both pore ends, matching the pressure field emerging in reaction to these forces (see Fig. 3, middle panel). We then solve the Stokes equation to predict the resulting flow.

The effective local pressure at either pore end is estimated by area averaging the axial electric body force, assuming it is fully present only in an annular region of width λ_D—corresponding to the EDL—with an axial extension comparable to the pore radius. For the step potential, this yields a time-dependent pressure at a pore end i of

$$P_i(t) = \frac{r_i^2 - (r_i - \lambda_D)^2}{r_i} \tilde{\rho}_v (1 - e^{-t/\tau_i}) \tilde{E}_{z,i} e^{-t/\tau_l}, \quad (3)$$

where we use tildes to denote characteristic scales and assume exponential decay on each timescale, due to the capacitorlike charging of the EDL [48]. Clearly, this pressure is higher at the narrow end of the pore. We estimate the characteristic volume charge via the Debye-Hückel approximation as $\tilde{\rho}_v \sim 2\zeta_0 c_0 F^2/(eRT)$, with temperature T and the Faraday and gas constants F and R, respectively. (See SM for details [38]). Assuming, again, that the electric field at both pore ends first emerges on a length scale comparable to the pore diameter (Fig. 3) yields $\tilde{E}_{z,i} \sim \zeta_0/(2r_i)$. The pressures in Eq. (3) are proportional to the multiplied step responses of volume charge and axial electric field. We find the time-dependent pressures in response to an ac gate potential $\zeta(t) = \zeta_0 \sin(\omega t)$ from these step responses [49] and again area average their product (see SM [38]):

$$P_i(t,\omega) = K_i \zeta_0^2 \frac{\omega\tau_l}{\sqrt{1+\omega^2\tau_i^2}\sqrt{1+\omega^2\tau_l^2}} \frac{1}{2} \left\{ \cos\left[\operatorname{atan}(\omega\tau_i) - \operatorname{atan}\left(\frac{1}{\omega\tau_l}\right)\right] - \cos\left[2\omega t + \operatorname{atan}(\omega\tau_i) + \operatorname{atan}\left(\frac{1}{\omega\tau_l}\right)\right]\right\}, \quad (4)$$

$$K_i = c_0 \frac{F^2}{eRT} \frac{r_i^2 - (r_i - \lambda_D)^2}{r_i^2}, \qquad i = n, w. \quad (5)$$

The first term in braces is a frequency-dependent constant offset and the second term describes a harmonic oscillation with twice the driving frequency and a frequency-dependent phase shift. To translate the effective pressures at the pore ends into a flow rate, we analytically solve for the pressure-driven flow in a conical pore under the long-wavelength approximation, yielding (see SM [38])

$$Q = -\frac{3}{8}\frac{\pi}{\mu} \frac{\frac{r_w - r_n}{L} r_n^3}{1 - \frac{r_n^3}{r_w^3}} (P_w - P_n), \quad (6)$$

where μ is the dynamic viscosity of the liquid. The resonance frequency ω_{res} readily follows from this expression by (numerically) solving $\partial\bar{Q}/\partial\omega = 0$ for $\omega > 0$. Overall, Eqs. (4)–(6) [Eqs. (3) and (6)] represent a full analytical model of the flow rate through the conical nanopore for a harmonic [steplike] gate potential, which does not contain any free parameters. The model is expected to make valid predictions if $\zeta_0 \ll RT/F$ and $\lambda_D < r_i \ll L$.

Comparison between model and numerical simulations.—Let us now systematically test the model by comparing it to our numerical simulations. Therefore, we compare the maximum flow rate $Q_{\max}$ and the time where this maximum occurs $t_{\max}$ for step response simulations [Fig. 4(a)] in a five-dimensional parameter space with $\zeta_0 \in \{1, 10, 100\}$ mV, $c_0 \in \{1.827, 3.653, 36.53, 182.7\}$ mol m^{-3}, $r_n \in \{7.5, 15\}$ nm, $L \in \{50, 100, 200\}$ nm, and $\alpha \in \{5, 10, 20\}°$, yielding $0.95 \geq \lambda_D/r_n \geq 0.048$. We note that $\lambda_D = 0.71$ nm at the highest concentration likely exceeds the scope of continuum theory. The result shows a good agreement over the entire parameter space [Fig. 4(c)], even for $\zeta_0 = 100$ mV > 25 mV $\approx RT/F$, which is beyond the regime where our assumptions are justified. Moreover, the pumping is not limited to certain EDL thicknesses.

Note that due to the linearity of the underlying charging processes, the comparison for the step response is largely representative also for the harmonic gate potential. As exemplarily shown in Fig. 4(b), the model correctly predicts the mean flow rate up to the resonance frequency. Noticeable deviations at larger frequencies can be attributed to the fact that the model assumes that driving axial fields at the pore ends are only governed by the delay of screening charge at the pore center (timescale τ_l). However, at high frequencies, the pore center remains uncharged at all times and otherwise negligible variations due to the local dynamics of charge generation at the corners (timescale τ_i) become dominant. This introduces nonlinearities that are not included in the model.

Experimental feasibility.—Several studies have proven manufacturability of gated nanopores [12,50] including conical shapes of similar dimensions as previously discussed [18,51]. The proposed mode of resonant ac driving is thus practically realizable. Moreover, it is not limited to the pore dimensions considered above, since the fundamental physical mechanism applies more broadly.

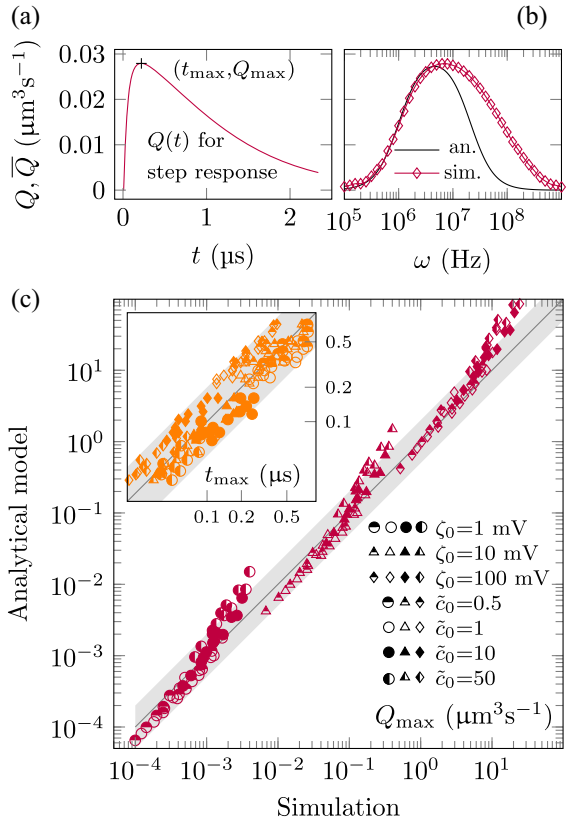

FIG. 4. (a) Step response of the system. (b) Mean flow rate $\bar{Q}$ over ac driving frequency for the analytical model and simulations; symbols denote time-domain simulations of governing equations. (a),(b) $\zeta_0 = 10$ mV. (c) Scatter plots comparing analytical and simulation results over a large domain of the parameter space for step responses, using the maximum flow rate Q_{max} and time of maximum flow rate t_{max} (inset), with shaded factor-two error areas and $\tilde{c}_0 = c_0/3.653$ mM.

Conclusions and outlook.—To conclude, we have demonstrated that electrolyte-filled conical nanopores with gate electrodes create a net flow when an ac voltage is applied to the gate. We have explained the emergence of a net flow as a resonance phenomenon that is based on two competing charging timescales. Achievable flow velocities range from millimeters to centimeters per second, which is comparable to electro-osmotic flow in nanochannels and other nanopumping principles [52–58]. Resonant nanopumping could allow real-time flow regulation in individually addressable nanopores, where the voltage amplitude and driving frequency serve as parameters to control the magnitude and temporal structure of the flow field. Generally, gated transport through nanopores under ac driving could open up superior possibilities for selective mass transfer, like in the case of macromolecules or nanoparticles. As an example, the principle could prove beneficial for controlling DNA translocation in sequencing applications. Last but not least, the nanopumping induced by transient EDLs uncovered in this Letter could find applications with a number of different electrode structures beyond conical shapes.

We wish to acknowledge the help provided by Maximilian T. Schür in preparation of the figures. S. H. and B. L. proposed the work, A. D. R. and D. P. carried out the simulations, A. D. R. developed the theoretical framework and the analytical model, A. D. R., B. L., and S. H. contributed to the interpretation of the results, A. D. R., B. L., and S. H. prepared the manuscript, and S. H. and S. B. supervised the work. S. B. acknowledges the financial support received from the Science and Engineering Research Board, Govt. India, under Grant No. MTR/2021/000020.

*benno.liebchen@pkm.tu-darmstadt.de
†hardt@nmf.tu-darmstadt.de

[1] D. Zhang and X. Zhang, Small **17**, e2100495 (2021).
[2] M. Rahman, M. J. N. Sampad, A. Hawkins, and H. Schmidt, Lab Chip **21**, 3030 (2021).
[3] M. Wanunu, Phys. Life Rev. **9**, 125 (2012).
[4] Y. Feng, Y. Zhang, C. Ying, D. Wang, and C. Du, Genomics, Proteomics Bioinf. **13**, 4 (2015).
[5] S. Wang, L. Yang, G. He, B. Shi, Y. Li, H. Wu, R. Zhang, S. Nunes, and Z. Jiang, Chem. Soc. Rev. **49**, 1071 (2020).
[6] Y. Liu, Z. Zhang, and S. Wang, ACS ES&T Water **1**, 34 (2021).
[7] M. Macha, S. Marion, V. V. R. Nandigana, and A. Radenovic, Nat. Rev. Mater. **4**, 588 (2019).
[8] K.-G. Zhou, K. S. Vasu, C. T. Cherian, M. Neek-Amal, J. C. Zhang, H. Ghorbanfekr-Kalashami, K. Huang, O. P. Marshall, V. G. Kravets, J. Abraham, Y. Su, A. N. Grigorenko, A. Pratt, A. K. Geim, F. M. Peeters, K. S. Novoselov, and R. R. Nair, Nature (London) **559**, 236 (2018).
[9] P.-c. Yen, C.-h. Wang, G.-J. Hwang, and Y. C. Chou, Rev. Sci. Instrum. **83**, 034301 (2012).
[10] Y. Liu and L. Yobas, ACS Nano **10**, 3985 (2016).
[11] L. Xue, P. Cadinu, B. Paulose Nadappuram, M. Kang, Y. Ma, Y. Korchev, A. P. Ivanov, and J. B. Edel, ACS Appl. Mater. Interfaces **10**, 38621 (2018).
[12] R. Karnik, R. Fan, M. Yue, D. Li, P. Yang, and A. Majumdar, Nano Lett. **5**, 943 (2005).
[13] M. Fuest, C. Boone, K. K. Rangharajan, A. T. Conlisk, and S. Prakash, Nano Lett. **15**, 2365 (2015).
[14] M. Fuest, K. K. Rangharajan, C. Boone, A. T. Conlisk, and S. Prakash, Anal. Chem. **89**, 1593 (2017).
[15] C. Cheng, G. Jiang, G. P. Simon, J. Z. Liu, and D. Li, Nat. Nanotechnol. **13**, 685 (2018).
[16] C. E. Ren, M. Alhabeb, B. W. Byles, M.-Q. Zhao, B. Anasori, E. Pomerantseva, K. A. Mahmoud, and Y. Gogotsi, ACS Appl. Nano Mater. **1**, 3644 (2018).
[17] Y. Xue, Y. Xia, S. Yang, Y. Alsaid, K. Y. Fong, Y. Wang, and X. Zhang, Science **372**, 501 (2021).
[18] E. B. Kalman, O. Sudre, I. Vlassiouk, and Z. S. Siwy, Anal. Bioanal. Chem. **394**, 413 (2009).
[19] W. Guan, R. Fan, and M. A. Reed, Nat. Commun. **2**, 506 (2011).

[20] G. Laucirica, W. A. Marmisollé, M. E. Toimil-Molares, C. Trautmann, and O. Azzaroni, ACS Appl. Mater. Interfaces **11**, 30001 (2019).
[21] J. Li and D. Li, J. Colloid Interface Sci. **596**, 54 (2021).
[22] P. Apel, Y. Korchev, Z. Siwy, R. Spohr, and M. Yoshida, Nucl. Instrum. Methods Phys. Res., Sect. B **184**, 337 (2001).
[23] A. R. Poggioli, A. Siria, and L. Bocquet, J. Phys. Chem. B **123**, 1171 (2019).
[24] W. Boon, T. Veenstra, M. Dijkstra, and R. van Roij, Phys. Fluids **34**, 101701 (2022).
[25] C. Wei, A. J. Bard, and S. W. Feldberg, Anal. Chem. **69**, 4627 (1997).
[26] Z. Siwy, Y. Gu, H. A. Spohr, D. Baur, A. Wolf-Reber, R. Spohr, P. Apel, and Y. E. Korchev, Europhys. Lett. **60**, 349 (2002).
[27] Z. Siwy and A. Fuliński, Phys. Rev. Lett. **89**, 198103 (2002).
[28] P. Jin, H. Mukaibo, L. P. Horne, G. W. Bishop, and C. R. Martin, J. Am. Chem. Soc. **132**, 2118 (2010).
[29] Ajdari, Phys. Rev. E **61**, R45 (2000).
[30] B. Matejczyk, M. Valiskó, M.-T. Wolfram, J.-F. Pietschmann, and D. Boda, J. Chem. Phys. **146**, 124125 (2017).
[31] A. Liakopoulos, F. Sofos, and T. Karakasidis, Phys. Fluids **29**, 052003 (2017).
[32] D. J. Bonthuis, D. Horinek, L. Bocquet, and R. R. Netz, Phys. Rev. Lett. **103**, 144503 (2009).
[33] K. F. Rinne, S. Gekle, D. J. Bonthuis, and R. R. Netz, Nano Lett. **12**, 1780 (2012).
[34] P. Reimann, Phys. Rep. **361**, 57 (2002).
[35] P. Hänggi and F. Marchesoni, Rev. Mod. Phys. **81**, 387 (2009).
[36] S. Denisov, S. Flach, and P. Hänggi, Phys. Rep. **538**, 77 (2014).
[37] S. Flach, O. Yevtushenko, and Y. Zolotaryuk, Phys. Rev. Lett. **84**, 2358 (2000).
[38] See Supplemental Material at http://link.aps.org/supplemental/10.1103/PhysRevLett.129.264501, which includes Refs. [39,40], for animated simulation results, for details, verification and validation of the numerical method, and for intermediate steps in derivation of the analytical model.
[39] R. F. Probstein, *Physicochemical Hydrodynamics* (John Wiley & Sons, Inc, Hoboken, NJ, 1994).
[40] A. A. Siddiqui and A. Lakhtakia, Appl. Math. Mech. **34**, 1305 (2013).
[41] V. G. Levich, *Physiochemical Hydrodynamics* (Prentice-Hall, Englewood Cliffs, NJ, 1962).
[42] J. R. Leigh, *Control Theory*, 3rd ed., IEE Control Engineering Series Vol. 72 (Institute of Electrical Engineers, London, 2012).
[43] M. Mirzadeh, F. Gibou, and T. M. Squires, Phys. Rev. Lett. **113**, 097701 (2014).
[44] M. Z. Bazant, K. Thornton, and A. Ajdari, Phys. Rev. E **70**, 021506 (2004).
[45] F. Henrique, P. J. Zuk, and A. Gupta, Soft Matter **18**, 198 (2021).
[46] T. Aslyamov and M. Janssen, Electrochim. Acta **424**, 140555 (2022).
[47] J. Yang, M. Janssen, C. Lian, and R. van Roij, J. Chem. Phys. **156**, 214105 (2022).
[48] M. Janssen, Phys. Rev. Lett. **126**, 136002 (2021).
[49] K. Berns, A. Köpper, and B. Schürmann, *Technical Foundations of Embedded Systems* (Springer International Publishing, Cham, Switzerland, 2021), Vol. 732.
[50] P. Joshi, A. Smolyanitsky, L. Petrossian, M. Goryll, M. Saraniti, and T. J. Thornton, J. Appl. Phys. **107**, 054701 (2010).
[51] S.-W. Nam, M. J. Rooks, K.-B. Kim, and S. M. Rossnagel, Nano Lett. **9**, 2044 (2009).
[52] A. Alizadeh, W.-L. Hsu, M. Wang, and H. Daiguji, Electrophoresis **42**, 834 (2021).
[53] R. Peng and D. Li, Nanoscale **8**, 12237 (2016).
[54] R. Qiao and N. R. Aluru, J. Chem. Phys. **118**, 4692 (2003).
[55] Z. Guttenberg, A. Rathgeber, S. Keller, J. O. Rädler, A. Wixforth, M. Kostur, M. Schindler, and P. Talkner, Phys. Rev. E **70**, 056311 (2004).
[56] S. Eloul and D. Frenkel, Soft Matter **17**, 1173 (2021).
[57] X. Zhang, X. Han, S. Qian, Y. Yang, and N. Hu, Anal. Chem. **91**, 4600 (2019).
[58] Y. Jin, X. Gao, K. Zhang, and Z. Li, Phys. Fluids **33**, 082001 (2021).

Correction: The previously published Figs. 1 and 4 reflected incorrect axis scalings and have been replaced. The Supplemental Material has also been replaced to correct for a corresponding error in Fig. S3.